Research Article

Ivan Azarov*

Reticular network as the Lymph Nodes railroad system: T cells migration modeling by the free energy minimization technique

https://doi.org/10.1515/rnam-2025-0015
Received Nov 13, 2023; revised Dec 31, 2023; accepted Feb 07, 2025

Abstract: One of the most important structural and functional elements of lymph nodes (LN) is the fibroblasts reticular network (RN). Placed *in vivo* in the LN space, lymphocytes can move directionally, in fact, just along the RN, which acts as a central immune highway. However, despite the multiple experimental studies, mechanisms regulating the lymphocytes motion are not fully understood. In this paper, we propose a modeling study of the basic mechanisms of the lymphocyte's migration along the reticulum's linear part at the subcellular level. Model simulations were performed in order to test several possibilities of the stochastic T cells motion along the RN driven by chemotaxis. The main goal of the work was to answer the question, what mechanisms are required to provide persistent and non-detached T cells gliding along whole length of the fibronectin fiber, maintaining the T cell integrity, using free energy minimization technique – Cellular Potts Modeling. As a result, a wide range of possible hypotheses and various CPM Hamiltonians were tested. The spatial chemokine gradient is not a universal solution to the problem. The linear chemokine gradient (haptotaxis) of the concentration distributed along the fiber does not solve the problem. Additionally, the production of chemokines by FRC fibers and their diffusion from the fiber into the lymph is not enough for a satisfactory solution as well. According to the proposed model, biologically relevant description of immune cells gliding along the RN can be achieved via a combination of haptotaxis and a spatially distributed gradient without a component normal to the fiber. The spatially distributed chemokine's gradient becomes a successful solution in combination with the active type of cell motion and fibronectin fibers defined as spatial corridors, which in fact is in line with various experimental evidence.

Keywords: cell motility, cellular Potts model, cell adhesion, chemotaxis, haptotaxis, reticular fiber

List of abbreviations:
ABM – Agent-based modeling
APCs – Antigen-Presenting Cells
CA – Cellular Automata
CPM – Cellular Potts Modeling
DC – Dendritic Cells
ECM – Extra-cellular matrix
FRC – Fibroblast Reticular Cells
HEV – High-Endothelial Venules
LN – Lymph Node
MCS – Monte Carlo Step
PFM – Phase-Field Modeling
RN – Reticular Network

***Corresponding author: Ivan Azarov,** Modeling & Simulation Decisions FZ-LLC, Department of Pharmacometrics, Dubai, United Arab Emirates, e-mail: ivan.azarov@msdecisions.tech

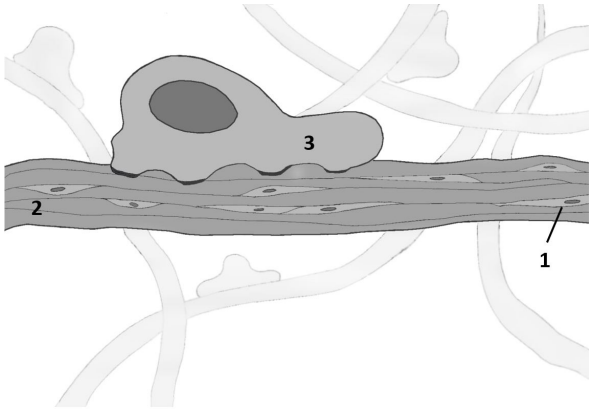

Fig. 1: T cell gliding along FRC network. 1 – fibroblast, 2 – reticular fiber, 3 – T-lymphocyte.

1 Introduction

1.1 T cells migration biology

It is well known that inflammation can dramatically enlarge a lymph node (LN) in several days. Therefore, the structural basis of the LNs cannot be too rigid; otherwise, it would prevent their rapid expansion. Rather, the "skeleton" of the LNs should resemble a web in its properties. This structural basis is established *via* Fibroblast Reticular Cells (FRC) network. Widely used approach of vital microscopy – 2-photon measurements demonstrate, that in their native conditions, T cells achieved their maximal velocities of more than 25 μm/min, displaying a motility coefficient (analogous to a diffusion coefficient), with values of 67 μm^2/min, [1]. Most of T cells moved by a series of repeated relatively stochastic lunges, becoming elongated while moving rapidly and balling up when paused [1]. Several less frequent patterns of T cell motility and shape included rapidly moving cells with torpedo shapes, a number of posterior visualizations suggested the presence of fibronectin fibers in these areas. Next observation is more general: lymphocytes adapt their motility to the composition of extra-cellular matrix, slow persistent walks correspond to collagen IV, and quick Brownian walks can occur in the fibronectin environment. At high cell density, collagen IV favored the self-assembly of lymphocytes into clusters, while fibronectin fibers caused individual motility [2].

Fibroblasts secrete collagen, which forms reticular fibers, filamentous structures with a diameter of less than 1 micron (fig.1). The reticular fibers are stitched together and form a web-like structure. The collagen network remains intact even after the destruction of the parental fibroblasts. Small molecules and antigens can spread inside the LN through a system of channels formed by reticular fibers. Cytokines and chemokines responsible for T cell migration, as well as nitric oxide, which inhibits T cell proliferation, are produced by the FRCs [3]. The inner part of the FRC network brings the antigen to the resident Dendritic Cells (DC), directing the lymph flow, while the outer part of the FRC network maintains and directs the motility of lymphocytes, participating directly in migration control [4].

In the LN, B cells migrate into the follicles while T cells remain in paracortex, with each type of lymphocyte showing apparently random migration behavior within these distinct areas. FRC network surrounding the High-Endothelial Venules (HEV) limits the output of T cells. After crossing this cellular barrier, T cells glide along the fibers to migrate to paracortex. An interesting fact is that network of fibronectin fibers separates T and B cell zones. B cell follicles are divided by FRC network and T cells cannot enter there. B cells migrate through the follicles along the network of dendritic cells (FDCs) developed there. B cells are attracted there by the CXCL-13 chemokine [5]. Thus, the migration of T cells within the LN is an intricate superposition of random and directed types of cell migration. In turn, experiments have shown that chemokines such as CCR7 ligands, CCL19 and CCL21, are released by the FRC and which in turn directly affect T cell motility. As the cell slides along the fibroblastic reticular fibers, the speed increases

by the beta factor (from 1.5 to 2.5). In the dense network scenario, the probability of contact between T cells and DCs increases with higher cell velocities [6]. The fiber routes and attracting chemokines signals combination organize quasi-fluxes of naive T cells to Antigen-Presenting Cells (APCs) which accelerate and promote T cell activation processes. In particular, the primed Ag-bearing DCs that initiate T cell activation during an immune response also cause FRC network relaxation, which allows space for T cell influx and more intensive trafficking [7].

In fact, cell migration is a complex process precisely regulated by a variety of receptors, crosslinking, binding, adhesive and motor proteins. These proteins help to set the direction of cell migration and adhering to the substrate and to accurately carry out events that determine the nature of migration. Cell gliding on the substrate is a cyclic process, largely due to actin polymerization and actomyosin contractility. In the absence of external stimuli, cell crawling consists of three main stages [8]: (1) forming a protrusion (lamellipodia, which are broad and flat, or filopodia, which are finger-like protrusions [9] in the direction of motion; (2) adhesion to the substrate at the leading edge and de-adhering the former protrusion in the back of the cell; (3) pulling the cell forward due to the contractile forces arising in the cell.

1.2 Mathematical models' overview

There are a variety of mathematical models describing various aspects of cell migration. In particular, subcellular models focus on the processes in a specific cell region or organoid: actin polymerization, blebs formation, actomyosin network dynamics or cell-substrate adhesion [10]. Cellular scale refers focus on the dynamics of membrane molecules, cytosolic components, or the combination of both [11]. The tissue-level models consider between-cell interactions and the trajectories of cellular migration within the tissue. The tissue-level continuous models operate on the cells and chemoattractant concentrations in a certain area. Individual-based models, which are able to describe individual cell behavior, can be further divided on on-lattice (Lattice gas, Cellular Automata, Agent-Based Modeling (ABM), Cellular Potts Modeling etc.) and off-lattice (Center-based, Vertex Models, Finite Elements, Front-tracking method, Voronoi diagrams and Phase Field modeling) approaches. Center-based models consider the continuous motion of discrete cells, which evolves under the control of force balance equations or energy functionals depending on the position of the center of mass [12]. Voronoi models better describe the cells shape and the cell size distributions due to their interactions [13]. Cellular Automata (CA) is the oldest on-lattice approach which formed a basis for many other modeling methods. The migrating cells are coded in CA by one lattice site, cell cycle phases and other variables are modeled via CA states. Phase-field modeling approach (PFM) reformulates the cell motion problem as a system of partial differential equations [14]. In this framework cell migration is viewed as a moving cell boundary problem.

At the same time, many model types use free energy minimization technique to describe the cells migration within tissues, e.g. geometrically similar to Voronoi models, Vertex models where cells form polygons [15]. A related front-tracking method approximates cellular contacts by discrete points moving according to a given evolutionary law [16]. The Finite Element method describe membrane tension using a constant force acting on point masses along each cell contact [17]. An on-lattice free energy formalism is presented by Cellular Potts Modeling (CPM) approach, where one cell occupies several lattice sites. The CPM and PFM are the most suitable for the description of cellular motion. Also, an advantage of the CPM is its high-resolution description of cell shapes compared with polygonal cells in vertex-based computations [18].

CPM is based on a free energy minimization technique. However, in particular cases, it could be more convenient to use forces acting on cells and cells' membrane explicitly [19]. Energy-based formalism is helpful to determine the direction of multicellular system's evolution. The dynamics are based on the free energy minimization principle [20], derived from First and Second laws of thermodynamics.

Another way to classify eukaryotic cell motion models by according to whether they describe cell deformations. First, in Cellular Automata, eukaryotic organisms formally have no size or just have some effective size. Second, in some Phase Field or Reaction-diffusion models, cells have a fixed geometry [21].

Center-based models may assume a fixed (or slightly deformable) cell geometry [14]. Third, the main feature of CPM or Vertex models consists of describing the variable shape of interacting cells [15]. If cell shape is not fixed, then there are multiple ways to determine the cells shape. The interface-tracking approach implies a scheme where the boundary is tracked explicitly: by Lagrange marker points [22], the immersed boundary method [23] or moving meshes [17]. The level set approach uses a time-varying distance function defined over a fixed region to determine the location of the cell membrane [16]. The PFM, from the other side, avoids use of moving meshes via inclusion of auxiliary field for identification of an area occupied by cell [14].

Rich variety of possible cell migration models can be classified as are they phenomenological or mechanistical models. Separate elegant types of theories are simple parsimonious models, which try to computationally explain different aspect of cells motility by the minimum number of equations according to Occam's razor principle. Thus, a simple but general model of cell gliding [24] is based on symmetry considerations. There, coherent resonance is used to create time-dependent forces. The nonlinear relationship between deformations significantly affects the crawling behavior. Subcellular and cellular scale models [10, 11] usually are rich on molecular aspects of cell motility details and add mechanistically plausible arguments to their framework. Tissue level models have often phenomenological character and try just to mimic the real systems avoiding any mechanistical features of cell motility [25]. At the same time other tissue level models can effectively reproduce, for example, actine polymerization processes, but in a simplified manner [26].

T cell migration processes have high impact on immune response initiation, therefore for the most modeling efforts it is very important to describe it with maximal biological sense and well-based assumptions. Recently, several detail solutions have been proposed for the implementation of actin-dependent cell migration at tissue level within the CPM framework [25–27]. However, it is still unclear whether such a modeling complication is really necessary and sufficient to create a phenomenological reproduction of lymphocyte migration along fibronectin fibers. Thus, the main objective of this study was in a reproduction of specific lymphocyte's migration along fibronectin fibers to imitate external features of gliding motion. Also, it was important to account for two possible motion types within one model: stochastic and directed motion. In order to address the following objective several quantitative hypotheses were formulated and tested within the CPM framework: (1) spatial chemokine's gradient, (2) linear gradient (haptotaxis), (3) haptotaxis, and two components of spatial gradient: tangential component along fiber and normal component attracting cell to the fiber, (4) haptotaxis and tangential component in layer of finite thickness (without pressing component), (5) spatial gradient and model of active protrusive cell motion with fibers as spatial corridors.

2 Computational methods

2.1 Cellular Potts Modeling as free energy minimization technique

To integrate individual cell's membrane deformations and migration processes into the model account, we use the CPM approach, a spatial grid-based formalism that allows cell description on the tissue level, where cells are defined as a region, composed of multiple square lattice sites [28].

The space discretization introduced in the model via immobile "sites". These sites can change their belonging to a particular biological cell or extracellular matrix (described by an index), according to the physically-based laws of evolution. The sites can be compared with Cellular Automata's cells. Each site is assigned a single cell index value $\sigma(\mathrm{i}, \mathrm{j})$. Biological cells are composed of all sites with the same index σ: usually several tens or hundreds of sites per cell. The further behavior of the system is described using the Potts Hamiltonian, the effective function of the total energy. "Effective" in this case means that not all energy types are taken into account. Some authors have also used the "free energy" term instead of "Hamiltonian", which in this framework assume equivalent.

The basic Hamiltonian proposed by Glazier and Graner [28] always includes the surface energy term of interaction between cells (1).

$$\mathcal{H}_{Potts} = \sum_{(i,j)(i',j'))} (1 - \delta_{\sigma(i,j)\sigma(i',j')}) \tag{1}$$

Summation is carried out on neighboring sites, not biological cells. From the definition of the Kronecker symbol, it follows that the interaction energy of sites with the same cell index equal to 0. Surface energy is proportional to the area of contact between sites belonging to different cells (with different indexes σ). The cell consists of all sites with the same index, therefore, the interaction energy of sites inside the cell is zero. As it can be seen, Equation (1) is valid only for the system with one cell type.

In order to account for the interactions between various cell types the Hamiltonian should be modified as follows (2):

$$\mathcal{H}_{\tau} = \sum_{(i,j)(i',j'))} [J(\tau(\sigma)), J(\tau(\sigma'))](1 - \delta_{\sigma(i,j)\sigma(i',j')}). \tag{2}$$

Here, not only different cells are introduced, but also different cell types. τ, τ' – different types of cells (2–5 different types per model): for example, in the current model 3 cell types are used: T cell, FRC and medium. J(τ, τ') is the surface energy of interaction between sites that belong to cell types τ and τ'. In general, J(τ, τ') is a symmetrical matrix, since the specific energy does not depend on the order in which cell types are mentioned. Of course, τ and τ' may have the same value.

It is also important to consider how constraints on the area, perimeter, or characteristic cell length are implemented within the energy formalism framework and respective Hamiltonian. According to Hooke's law, the elastic energy of area deviation from the target values must contain this term in square form (3):

$$\mathcal{H}_{Modified} = \mathcal{H}_{\tau} + \lambda \sum_{\sigma} [a(\sigma) - A_{\tau(\sigma)}]^2. \tag{3}$$

Here, the summation is over the indexes σ (that is, over separate biological cells). λ – Lagrange multiplier responsible for the strength of the area constraints effect. a(σ) – current cell area σ. $A_{\tau(\sigma))}$ – target cell area σ.

A term of the similar type was also used for cell perimeter constraints. It should be clarified that an area of a particular cell is considered as the sum of all sites of the corresponding cell index. However, the perimeter is calculated differently: in the cycle for all border sites, the sums of neighbors with other cell indexes in the von Neumann neighborhood (only 4 sites) with a radius of 1 were considered. The present model uses a T cell with a target area of 300 sites and a target perimeter of 100.

Important to note, that in term of the system behavior a Hamiltonian change from the previous step is more meaningful rather an its absolute value:

$$\Delta\mathcal{H} = \mathcal{H}_{after} - \mathcal{H}_{before}, \tag{4}$$

which in turn determines the further evolution of the system.

The Hamiltonian only includes static cell properties such as area, perimeter and neighbors. To include dynamic cell behavior, such as chemotaxis, extra terms may be added to the Hamiltonian change $\Delta\mathcal{H}$ [58]. In order to account that migration along the chemokine gradient is more energy-efficient, the $\Delta\mathcal{H}$ can be modified according to chemotaxis term proposed in [29]:

$$\Delta\mathcal{H}' = \Delta\mathcal{H} + \lambda_{chem}(c(x) - c(x')). \tag{5}$$

The Equation (5) is relevant for the chemoattraction, when the cell moves along the chemokine's gradient. And it is used for calculation of the probability of index copying from site x to x'. Thus, a concentration of c(x') greater than c(x) leads to an increase in the probability of the corresponding migration on microlevel.

The same term (5) can be used for the description of the cell guidance by anchored molecules, or haptotaxis. Adhesive haptotaxis, or guidance by adhesion molecules, is well established for mesenchymal cells such as fibroblasts, however it was also reported recently for the amoeboid human T lymphocytes which

develop adhesive haptotaxis mediated by densities of integrin ligands VLA-4 expressed by high endothelial venules [30]. Other leukocytes also exhibit haptotactic motion: neutrophils undergo IL-8-mediated migration, while monocytes, basophils, eosinophils and some T cells are influenced by RANTES (CCL5) chemokines [31]. Also, Marc Bajenoff and co-authors [5] proposed in their work an important hypothesis, that by localizing particular chemokines to stromal cells, haptotactic rather than chemotactic guidance cues may promote proper lymphocyte localization and guidance of trafficking within LN subregions.

To carefully land the T cell on the fibronectin fiber under the same conditions we used an additional correction to the Hamiltonian, which was turned off after the T cell touches the fiber. This correction corresponds to a directed migration along a certain force of a general nature. In a simplified situation, the vector of external force $\overrightarrow{F^M}$ can be replaced by a constant vector of the preferential direction. The functional form of the correction (6) was initially proposed by Guisoni [25]:

$$\Delta\mathcal{H} = \Delta\mathcal{H}_0 + \sum_{M=1}^{Q} \overrightarrow{F^M} \cdot \overrightarrow{\Delta r^M}, \tag{6}$$

where $\Delta\mathcal{H}_0$ is the change of energy due to Equation (4) or $\Delta\mathcal{H}$' in the presence of chemotaxis from Equation (5), the M index corresponds to the separate biologic cell, if there is only one cell in the system, then summation over M is not required.

In the program code, the correction was included via the scalar product of the random force direction and the displacement vectors. The correction is applied not to a separate site where the index is copied, but to the center of mass of a biological cell (one of Q cells).

The Equation (6) can be used to describe active cytoskeletal motion of cells. In such case the absolute value of driving force $\left|\overrightarrow{F^M}\right|$ will be constant. And direction of a driving force $\overrightarrow{F^M}$ updates according to solution (7) of stochastic differential equation proposed by Guisoni [25] in the Euler-Maruyama form [32]:

$$\Theta(t^*) = \phi \cdot \Theta(t^* - 1) + \Delta\Theta \cdot \epsilon(t^*), \tag{7}$$

where t^* means the current time step, $\Theta(t^* - 1)$ indicates the direction previous to the actualization time. Percentage of the previous step's angle value that remains for the next step – ϕ and maximum value of deviation from the previous step angle value – $\Delta\Theta$ are constant parameters, that can take values between $(0, 1)$ and $(0, \pi)$, respectively. $\epsilon(t)$ is a white noise process with zero mean and unit variance ($\sigma_\epsilon^2 = 1$). The equation (7) can be rewritten in terms of the Ornstein-Uhlenbeck process with media zero (8):

$$dx(t) = -\lambda x(t) - \sigma dW(t), \tag{8}$$

where $dW(t)$ denotes a stochastic Wiener process and x means random force direction here. And setting the friction coefficient $\lambda = (1 - \phi)$ and $\sigma = \Delta\Theta$, equation (7) becomes the discrete-time translation of the Ornstein-Uhlenbeck process [25].

Thus, the cell's persistence time is characterized by ϕ, $\Delta\Theta$ and characteristic time τ. The initial angle of the cell, $\Theta(0)$, is chosen randomly. At each Monte Carlo step (MCS) the driving force direction for each cell changes with probability $1/\tau$ according to Equation (7). Thus, the change in a driving force direction Θ occurs at a mean time τ.

There are several ways to introduce a positive feedback loop in cell polarization dynamics, when cell protrusions reflect the dynamics on previous steps [27]. In order to take into account this feedback loop, an alternative form of Eq. (7) can be taken to update the angle Θ [33]:

$$\Theta(t^*) = \phi \cdot \overline{\alpha(t^* - 1)} + \Delta\Theta \cdot \epsilon(t^*), \tag{9}$$

where $\overline{\alpha(t^* - 1)}$ is the mean angle of the accepted cells displacements over the last τ MCS. Way, proposed in eq. (9), links random force direction and the mean direction of persistent cells motion in a stochastic way.

The evolution dynamics within CPM framework is based on the free energy minimization principle [20, 34], and generated by means of Monte Carlo Simulations via the Metropolis algorithm [35]. Steps of

modified Metropolis algorithm [36] are presented below (step №3 was suggested by Sahni instead of step №2):

1) Selection of a random candidate site (i, j) with index σ.
2) Selection of a random new value of the index σ' from Q possible values.
3) Selection of a random new value of the index σ', with σ' chosen among the values of the neighbors.
4) Calculation of the energy of the system $\mathcal{H}_{after}$ in the new configuration.
5) Changing the cell index $\sigma(i,j)$ to σ':

Calculation of the transition probability at T > 0:

$$p(\sigma \to \sigma') = \begin{cases} e^{-\frac{\Delta\mathcal{H}}{kT}} & if\ \Delta\mathcal{H} > 0 \\ 1 & if\ \Delta\mathcal{H} \leq 0 \end{cases} \tag{10}$$

Or calculation of the transition probability at T = 0:

$$p(\sigma \to \sigma') = \begin{cases} 0 & if\ \Delta\mathcal{H} > 0 \\ 0.5 & if\ \Delta\mathcal{H} = 0 \\ 1 & if\ \Delta\mathcal{H} > 0 \end{cases} \tag{11}$$

In step 6, the calculated probability accounts for either accepting or rejecting a particular index copying. Usually, such a procedure is carried out by generating a uniformly distributed random number from 0 to 1. And if a random number is greater than $p(\sigma \to \sigma')$, the copying does not occur. If a random number less than $p(\sigma \to \sigma')$ is generated, the copying is accepted, and the site (i, j) gets a new index σ'.

To avoid misunderstandings, let us clarify: the selection of the candidate site and the new index value σ' occur with equal probability of all available options. Formulas for the probability calculation (10), (11) are applied to the selected option. And these formulas describe the probability of accepting the selected index copying.

The transition probability calculation in the Boltzmann form contains the temperature parameter. Its biological meaning was explored experimentally by the membrane oscillation inhibition using cytochalasin B, which partially or completely damages cell sorting. According to those results, cell membrane oscillations play a role similar to temperature in conventional materials, increasing the cells motility and allowing them to interact with their neighbors [37]. Consequently, the system can overcome energy barriers and explore energy space in order to reach its global minimum, therefore $T = 7$ was used.

2.2 Numeration algorithm

In order to account for chemokine's concentration setting process for any form of reticular fiber (FRC sites numeration) we used an algorithm similar to wave propagation, which can be described as follows:

1. N corresponds to the number of fiber sites.
2. Select one of the fiber sites with the maximum value of the linear concentration, $max(C_{lin})$.
3. Find a fiber neighboring site adjacent with a zero linear concentration.
4. Assign the value to linear concentration $max(C_{lin}) + 10$.
5. Return to step 2 (applied to the neighbors of the original patch).
6. The following procedure is repeated N times.

To clarify results of the described algorithm: the final result of the algorithm execution is the chemokine linear concentration C_{lin} gradually increasing along the fibronectin fiber length to make chemotaxis migration possible.

2.3 Local sensitivity analysis

To assess the effect of different model parameters on the T cell gliding along the fiber and, above all, on the transit time, the simplest version of Sensitivity Analysis was used – Local Sensitivity Analysis with

variation of each parameter separately. Local relative sensitivity indices (LSI) were defined as the ratio of the cell transit time increment to change in the studied parameter relative to the baseline value (12). To calculate the indices, all parameters were increased by 10% relative to the baseline value so that the sign of the effect was reliable against the significant internal variability of the stochastic system.

$$LSI = \frac{TT(\theta + \Delta\theta) - TT(\theta)}{\Delta\theta/\theta}, \tag{12}$$

where TT is the mean transit time, θ – baseline value of the studied parameter.

2.4 Software

To implement the tested hypotheses into the CPM framework, a specialized language and programming environment that operates with Cellular Automata and ABM, NetLogo 6.3.0 [38], was used. This allowed new models to be coded and tested by non-programmers. Statistical analysis was performed in R Statistics 4.2.2. To perform Sensitivity Analysis, it was necessary to run a large number of identical calculations, which were started in automatic mode with parallelization on several processor cores. For such calculations, the "BehaviorSpace" NetLogo extension was used. The mean time for one run of model №4 on a Lenovo ThinkPad (Intel Core i5-8265U CPU, 8 GB RAM) laptop was 40 seconds. One run of model №5 on a same laptop took 4 minutes 23 seconds. The duration of running models 2 – 3 cannot be estimated, since the condition for completing the calculations is not met there.

3 Numerical results

The main objective of the current work and the corresponding CPM modeling is to identify elementary mechanisms, i.e. in the language of CPM – Hamiltonians and their combinations, which are capable to provide non-detached and persisted gliding of T cells along fibronectin fiber, maintaining the T cell integrity. If the distance is not covered in compliance with the conditions, the hypothesis is rejected. The task was considered as failed in the next cases:

1) The T cell left and completely detached from the fibronectin fiber along which it should move;

2) The T cell did not reach the fiber section opposite to the starting one within a maximum time of 80000 ticks ($\approx 400MCS$);

3) The T cell fragmented during the gliding (maximum area loss – up to 30% of the target value);

4) Rare error examples: demonstration of extreme forms of non-biological behavior, for example, stretching of the T cell to a length of more than half the fiber.

All models used a computational domain of 120×60 pixels with impenetrable boundaries. The fibronectin fiber for models 1 – 4 is represented by 3 points connected by segments: (-60, -25), (0, -10) and (60, -25). Thus, the T cell must overcome the vertex (0, -10) during its gliding and not disconnect from fibronectin fiber.

The tested hypotheses are formulated in terms of (1) the biological mechanisms which are considered to be enabled or disabled and (2) by the particular CPM Hamiltonian parametrizations which are used to simulate the hypothesis. The list of tested hypotheses is provided in table 1.

The only quantifiable metrics of the desired model outcome is the T cell transit time from starting position to the finish along fiber (the fiber length was around 62 pixels) with the fulfillment of all listed conditions. However, the main modeling outcome is not a number, but the fact, that distance is overcome, i.e. models were not compared by resulting cell velocities or how close was the cell velocity to the experimental values. Simply, 80000 ticks were considered as the threshold for the transit time, and the distance was considered not covered if the time was greater than the threshold.

Tab. 1: List of tested hypotheses.

Hypotheses	Biological mechanisms	Hamiltonians
First	T cell adhesion to fiber and chemotaxis	(3), (5)
Second	T cell adhesion to fiber and haptotaxis	(3), (5)
Third	T cell adhesion to fiber chemo- and haptotaxis	(3), (5)
Fourth	T cell adhesion to fiber chemo- and haptotaxis	(3), (5)
Fifth	T cell adhesion to fiber, chemotaxis and actine-based protrusive motion	(3), (5), (6) - (9)

Fig. 2: First hypothesis: black line is the fiber; blue figure corresponds to T cell gliding along fiber.

3.1 First hypothesis

The first hypothesis tested was the mechanism of chemotaxis due to a spatially distributed chemokine gradient (Fig.2). Lymphocytes can indeed slide along the fiber due to chemokines dissolved in LN volume: directly *via* equation (5). An additional degree of physiological plausibility is achieved using the zero surface energy of T cells "sticking" to the FRC ($J_{cf} = 0$).

However, even such computational trick does not relieve from quite possible situations when the fiber is oriented at a certain angle relative to the driving force of chemotaxis. To reveal such possibility series of numerical experiments was carried out: 20 for each angle value. As a result, in the case of an angle between the linear section of the fiber and gradient direction is equal to 45 degrees: 15 times the lymphocyte passes the section completely, 5 times disconnected from the linear section and continues unnatural migration without connection to the fiber. At an angle of approximately 63.5° ($tan(\alpha) = 2$), the lymphocyte disconnected from the fiber 14 times and stopped moving 6 times, thereby hasn't passed the site even once.

In conclusion, we note that in some cases it is possible to use the already known term of spatial gradient as a driving force and FRC as a road network. However, from the algorithmic point of view, this solution is not generalizable. If the component normal to the fiber is large, then it can disconnect the lymphocytes from the network or slow them down. Apparently, the conclusion also has a biological meaning: it is impossible to describe all known types of migration along the FRC network using spatial chemotaxis. The final set of parameters used for the testing of the first hypothesis is presented in Table 2.

Despite the non-universality of the first hypothesis, a series of 20 runs of the model was carried out. The cell passed the entire fiber, without fragmentation, in 14 cases out of 20. On average, the calculated transit time, including cell adhesion on the fiber, spend 5.2 ± 0.44 min (13870 ± 1181 ticks) with mean gliding velocity $8.6\mu m/min$. To describe the fiber transit times, the mean ± standard error was calculated.

Parameter	Description	Value	Source
T	**Temperature in Boltzmann expression**	7	**Decreasing from [55, 57] to eliminate fragmentation**
λ_{per}	**Lagrange multiplier for perimeter**	1	**Starting from 2D case of [57]**
P_{Tcell}	**T cell target perimeter**	$50\mu m$	**Based on pixel size estimations from [56]**
λ_{Ar}	**Lagrange multiplier for area**	1	-
A_{Tcell}	**T cell target area**	$75\mu m^2$	**Based on pixel size estimations from [56]**
λ_{grad}	**Lagrange multiplier for chemotaxis**	10	**2D case of [57]**
J_{cm}	**Cell-medium surface energy**	1	-
J_{cm}	**Cell-fiber surface energy**	0	**LN simulations in [57]**

Tab. 2: Model parameter values used for the first hypothesis testing.

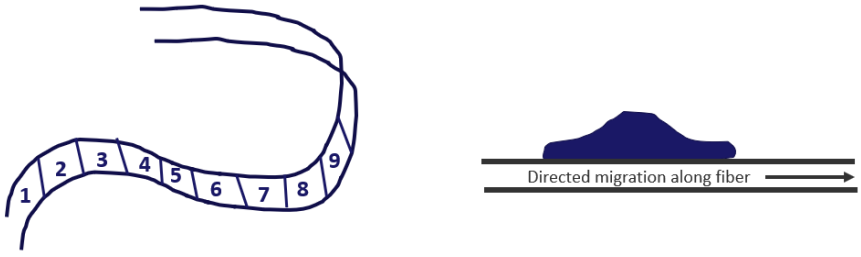

Fig. 3: Second hypothesis. Left: linearly distributed variable value according to the numeration algorithm. Right: black ribbon is the fiber; blue figure means T cell gliding along fiber.

3.2 Second hypothesis

The second tested hypothesis was using of the same Hamiltonian expression, eq. (5), but only for the haptotaxis mechanism along the length of a particular network fiber (fig.3). Variable change should suggest the preferred migration direction on the FRC network. By increasing the corresponding Lagrange multiplier, one can control the haptotaxis contribution compared to other forms of energy. It is possible to set the value of the linear concentration on the fiber using the previously described numeration algorithm (see section 2.2).

To test hypothesis 2, T cell was landed approximately in the middle of a linear fiber using a directional migration Hamiltonian that turned off after contact with the fiber. All other conditions were the same as in the first hypothesis testing ($T = 7$, $J_{cf} = 0$, *etc.*). All fiber patches from x = -60 to x = 60 were provided with a progressively increasing variable p_{num} from 0 to 14400. Thus, T cell gradually starts moving towards the x = 60 patch. The following variables were used to characterize the position of a lymphocyte on a numbered fiber:

$$num_i = \sum_{i=1}^{i=4} p_{num}, \tag{13}$$

num_i was used to describe T cell sites by summation of p_{num} values over neighboring fiber patches (von Neumann neighborhood).

$$MOVE_{index} = \sum_{i=1}^{i=N} num_i, \tag{14}$$

where N – full number of T cell sites. And the increase of the $MOVE_{index}$ should have led to the directed type of motion.

However, the actual result was quite different. On 20 out of 20 attempts, the T cell did not overcome the required distance to the right edge of the fiber in the allowed, obviously sufficient time – 80000 ticks. At the same time, the projection of the mass center on X axis was always around zero. The variable $MOVE_{index}$ (13) increased its value, but only due to the flattening of the T cell on the fiber.

The algorithm does not work, even for elementary cases of the FRC pixels numeration. From an algorithmic point of view, the new Hamiltonian acts only on the lymphocyte's sites adjacent to the fiber. The remaining pixels of the T cell "do not feel" haptotaxis since they do not encounter fiber. From a biological meaning, the chemokine gradient for oriented T cell gliding should be spatial, but at the same time localized along the fiber. That is, we are talking about either a near-surface layer of chemokine molecules, thanks to the diffusion laws, or about molecules localized in a system of branched filaments. The final set of parameters used for the testing of the second hypothesis is presented in Table 3.

Parameter	Description	Value	Source
T	**Temperature in Boltzmann expression**	7	**Decreasing from [55, 57] to eliminate fragmentation**
λ_{per}	**Lagrange multiplier for perimeter**	1	**Starting from 2D case of [57]**
P_{Tcell}	**T cell target perimeter**	$50\mu m$	**Based on pixel size estimations from [56]**
λ_{Ar}	**Lagrange multiplier for area**	1	-
A_{Tcell}	**T cell target area**	$75\mu m^2$	**Based on pixel size estimations from [56]**
λ_{hapt}	**Lagrange multiplier for haptotaxis**	10	**2D case of [57]**
J_{cm}	**Cell-medium surface energy**	1	-
J_{cm}	**Cell-fiber surface energy**	0	**LN simulations in [57]**

Tab. 3: Model parameter values used for the testing of the second hypothesis.

Fig. 4: Third hypothesis. Bold line on the bottom side– reticular fiber, arrows are normal and tangential parts of chemotaxis vector, irregular blue spot – migrating T cell.

3.3 Third hypothesis

The third hypothesis accounted that the haptotaxis affects not only the lymphocyte sites adjacent to the fiber, but also other sites. To implement this, the system was designed so that fiber sections emit chemokine molecules into space in proportion to their surface concentration. Thus, chemotaxis has been set both along the fiber and towards FRC fiber (fig.4).

When setting the spatial chemokine concentration, we haven't account in detail for the diffusion laws and accurate representation of a spatial concentration profile. In fact, we reproduced the effect of chemokine distribution away from the fiber on the discrete sites. The volume concentration for the fiber sites is identically equal to their linear concentration tested in the previous hypothesis. But the chemokine volume concentration of the remaining sites of the computational domain is calculated as the mean variable value over all neighbors from the Moore neighborhood of the first order.

$$num_i = \frac{1}{8}\sum_{i=1}^{i=8} num'_i, \tag{15}$$

where num'_i is volume concentration on neighboring sites. And such chemokine distribution calculations were made several iterations. It should also be noted that eq. (13) and (14) were still valid for hypothesis 3.

Third solution allows the lymphocyte to reach the opposite side of the computational area, on average, in 35000 ticks. However, this solution leads to incorrect unnatural behavior of the lymphocyte, e.g. multiple fragmentation during the simulation with area decrease more than 10%, flattening and stretching of the cell by more than half of the computational area. The possible explanation of those numerical results is that the normal gradient is much larger than the longitudinal one, and the T cell clings to the fiber and slows down. The final set of parameters used for the testing of the third hypothesis is presented in the Table 4.

3.4 Fourth hypothesis

The fourth hypothesis was based on the chemokine layer construction along the fibronectin fiber with concentration changing only along its length, but devoid of the normal component of the gradient (fig.5A).

Parameter	Description	Value	Source
T	Temperature in Boltzmann expression	7	Decreasing from [55, 57] to eliminate fragmentation
λ_{per}	Lagrange multiplier for perimeter	1	Starting from 2D case of [57]
P_{Tcell}	T cell target perimeter	$50\mu m$	Based on pixel size estimations from [56]
λ_{Ar}	Lagrange multiplier for area	1	-
A_{Tcell}	T cell target area	$75\mu m^2$	Based on pixel size estimations from [56]
λ_{chem}	Lagrange multiplier for chemotaxis	10	2D case of[57]
λ_{hapt}	Lagrange multiplier for haptotaxis	10	Equals to multiplier for chemotaxis
J_{cm}	Cell-medium surface energy	1	-
J_{cm}	Cell-fiber surface energy	0	LN simulations in [57]

Tab. 4: Model parameter values used for the testing of the third hypothesis.

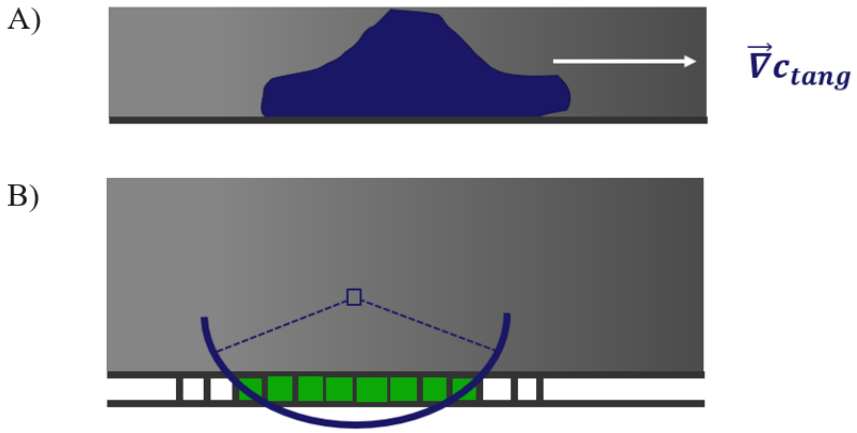

Fig. 5: Fourth hypothesis: A) bold line on the bottom side of the scheme – reticular fiber, arrow is chemotaxis vector, irregular blue spot – migrating T cell. B) Graphical representation of the chemokine concentration calculation. Green squares are sites where the linear chemokine concentration was taken into account.

The decision was made based on the main drawback of the third hypothesis, where the normal component of the gradient interfered with the migration along the fiber. The fact that a linear distribution of the chemokine concentration (i.e. haptotaxis) on the fiber is not enough for T cell migration is supported by the shortcomings of the second hypothesis as well.

However, the corresponding question is how to universally calculate the chemokine volume concentration based on the chemokine linear concentration for an arbitrary-shaped fiber. According to the descriptive geometry solutions the algorithm was chosen as follows: calculate the mean concentration over all fiber pixels in the neighborhood of a predefined radius – from a given pixel (fig.5B). Due to the finite radius length, the chemokine concentration layer itself was obtained. Indeed, chemokine molecules may not be dissolved in the lymph, but may sit on fiber irregularities, protruding filaments or on the membrane of fibroblasts, also located on the ECM fiber [39]. Additionally, it can be proposed that when chemokines are emitted from the reticular fiber, a thin surface layer of chemokine is formed, held by a "fur coat" of filaments.

The fourth hypothesis led to the final model with the oriented T cells migration along the reticular fiber. Of the 20 simulations tested, the lymphocyte reached the opposite side of the computational domain in 100% of cases. On average, the entire computational domain transit time, including cell adhesion on the fiber, spend 2.17 ± 0.02 min (5788 ± 45 ticks) with mean gliding velocity 20.7 $\mu m/min$. To describe the fiber transit times, the mean ± standard error was calculated. One can compare these times with over 80 000 ticks during hypothesis № 3 testing. During migration, the lymphocyte did not undergo fragmentation, although it gradually lost from the rear side around 10 10% of the area during gliding. An important issue revealed during the testing of fourth hypothesis that the volume concentration should be set once before calculations start, and not updated during the calculations since concentration recalculation dramatically

Parameter	Description	Value	Source
T	Temperature in Boltzmann expression	7	Decreasing from [55, 57] to eliminate fragmentation
λ_{per}	Lagrange multiplier for perimeter	1	Starting from 2D case of [57]
P_{Tcell}	T cell target perimeter	$50\mu m$	Based on pixel size estimations from [56]
λ_{Ar}	Lagrange multiplier for area	1	-
A_{Tcell}	T cell target area	$75\mu m^2$	Based on pixel size estimations from [56]
λ_{chem}	Lagrange multiplier for chemotaxis	10	2D case of [57]
λ_{hapt}	Lagrange multiplier for haptotaxis	10	Equals to multiplier for chemotaxis
J_{cm}	Cell-medium surface energy	1	-
J_{cm}	Cell-fiber surface energy	0	LN simulations in [57]

Tab. 5: Model parameter values used for the testing of the fourth hypothesis.

increases simulation time. The final set of parameters used for the testing of the fourth hypothesis is presented in Table 5.

Local sensitivity analysis based on the fourth hypothesis was performed to estimate partial effects of main model parameters. Below is an assessment of the role of individual parameters in the fourth model, illustrated by fig.6. The single parameter of directed motion due to the chemokine gradient (λ_{Hapt}) reduces transit time as the main outcome measure of numerical experiments. Increase of the T cell – environment surface energy (J_{cm}) also reduces the transit time, making the contact between the lymphocyte and the fiber denser, that is, allowing the haptotaxis mechanism to be fully realized. Perimeter constraints coefficient (λ_{Per}) has almost no effect on the transit time. It was also found that increasing surface energy (J_{cf}) of the lymphocyte interaction with the fiber slows down the cell gliding along the fiber, making the contact between T cell and fiber less dense. And the most interesting output is that, increasing the energetic contribution of elastic area constraints (λ_{Ar}) leads to an increase in transit time (and a decrease in velocity). It is quite possible that this numerical result echoes the conclusions obtained in [58], which indicate that an increase in λ_{Ar} reduces cell mobility, in the extreme case leading to that incompressible cells will be immobile within the CPM framework. Also, the transit time increases with increasing temperature (T). It can be assumed that temperature as a measure of the membrane oscillations energy is capable of disrupting the stable T cell – fiber contact and increasing the stochastic component of motion in this CPM configuration. Sensitivity index was also estimated for a dummy parameter that does not affect the model outcome, so that the model parameter sensitivity indices could be compared with the intrinsic variability of the simulation results with baseline parameters.

3.5 Fifth hypothesis

In the first published examples of the Cellular Potts Modeling, cell migration was considered because of membrane oscillations and rebuilding due to cell-cell or cell-medium interactions, or as a response to an external chemotactic gradient [29]. Recent findings have shown that eukaryotic cells can exhibit persistent displacements across scales larger than cell size, even in the absence of external stimuli [40]. Persistent cell motion has been implemented into the cellular Potts model by many authors [25–27] in the context of collective motion, chemotaxis and morphogenesis. Therefore, it has sense to test another hypothesis using active cytoskeletal motion to describe the T cells migration along fibronectin fibers.

However, active cytoskeletal motion implementation is poorly consistent with the description of fibronectin fibers as one-dimensional structure. In fact, FRC network represents rather spatial corridors than guiding threads or cable cars [41]. Therefore, in the fifth hypothesis, the geometry tested via hypothesis 4 was reproduced, but with modified rules. Here, the T cell can move exclusively within the gray ribbons corresponding to fibers (fig.7). Within the framework of the CPM, this means that the "recoloring" of sites can only occur from the FRC sites (grey) to the T cells (red) and *vice versa*, without the medium involvement (blue sites). Computational domain sizes and angles remain the same as in the previous models.

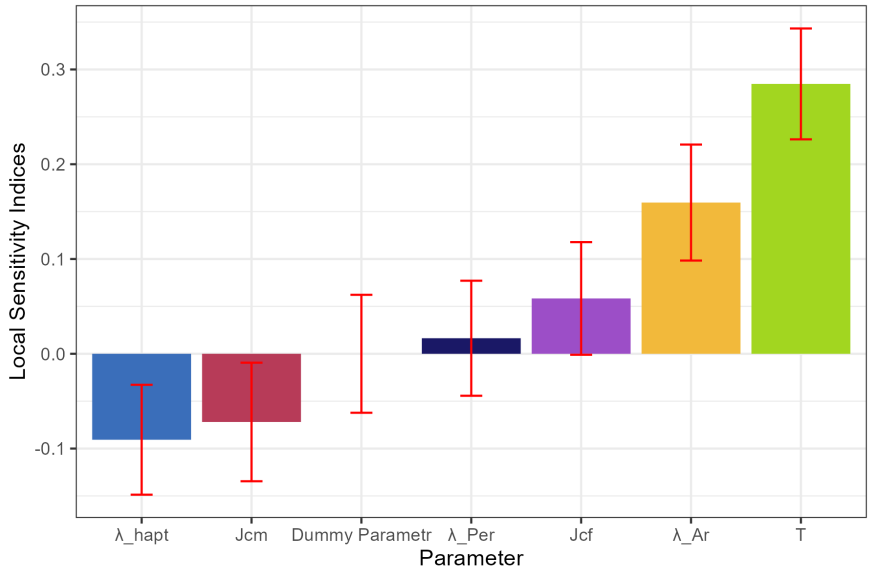

Fig. 6: Local sensitivity analysis of model №4 main parameters variation. The plot shows mean ± se for sensitivity indices based on 200 runs for all parameters.

Parameter	Description	Value	Source
T	**Temperature in Boltzmann expression**	7	**Decreasing from [55, 57] to eliminate fragmentation**
N_{iter}	**Number of ticks in 1 MCS**	200	**2 cell perimeters**
λ_{per}	**Lagrange multiplier for perimeter**	2	**[26, 57]**
P_{Tcell}	**T cell target perimeter**	$60\mu m$	**Based on pixel size estimations from [56]**
λ_{Ar}	**Lagrange multiplier for area**	10	-
A_{Tcell}	**T cell target area**	$75\mu m^2$	**Based on pixel size estimations from [56]**
λ_{chem}	**Lagrange multiplier for chemotaxis**	10	**2D case of [57]**
J_{cm}	**Cell-medium surface energy**	1	**2D case ECM value of [57]**
J_{cm}	**Cell-fiber surface energy**	0	**LN simulations in [57]**
λ_{Pr}	**Lagrange multiplier for active motion**	10	**[25]**
ϕ	**Remaining part of previous angle value**	0.95	**[25]**
$\Delta\Theta$	**Angle amplitude for noise term**	$\pi/3$	**[25]**
τ	**Characteristic time**	0	**[25]**

Tab. 6: Model parameter values used for the fifth hypothesis testing.

To introduce active type of cell motion Guisoni model was implemented in NetLogo code [25], Eq.(6) – (9). The final set of parameters used for the fifth hypothesis testing is presented in Table 6.

Some additional model assumption needs to be explained: only the fiber sites were included in index-copying exchange with the T cell sites. However, to prevent adhesion of the lymphocytes to fiber boundaries surface energy between T cell and medium J_{cm} was set higher than between T cell and the fiber (J_{cf}). Such implementation leads to the correct behavior, T cell does not stop in the turns or branching of the FRC network, trying to avoid a large contact area with the medium. To unify modelling process, standard form of Lagrange multiplier for active motion (λ_{Pr}) was used. The physical meaning of this multiplier is an absolute value of the random directed force $\left|\overrightarrow{F^M}\right|$ and was proposed previously by Nara Guisoni [25]. Another numerical feature of the fifth model was a measure of time in different units during calculations. In particular, due to the eqtions (7), (9), where the Θ angle should be modified every τ Monte Carlo Steps. Therefore, in this model, we do not use the usual NetLogo ticks to describe time and replace them with MCS. In the current work, 1 MCS = 200 ticks, that is, 2 cell perimeters – approximately the number of sites which index copying is theoretically possible for.

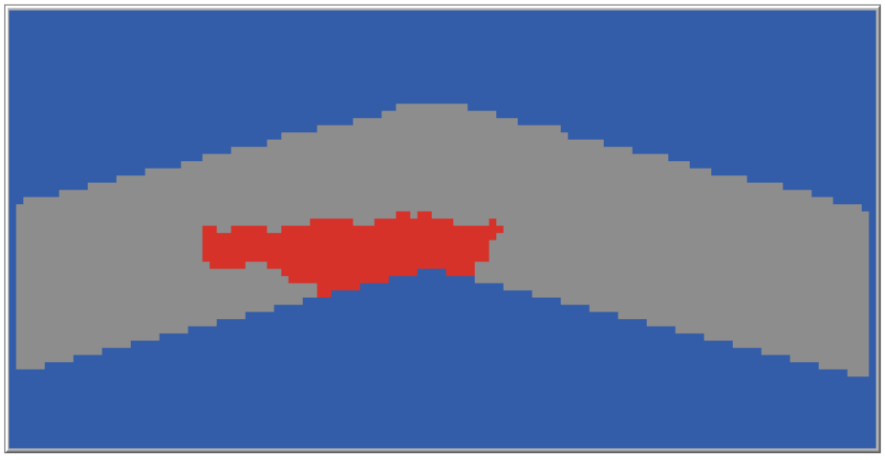

Fig. 7: Build-in NetLogo visualization of the computational domain used for the fifth hypothesis testing. Blue environment – medium, grey ribbon – FRC network fiber, red figure – migrating T cell.

The fifth hypothesis simulation led to the building of an alternative model for oriented T cells migration along the reticular fiber. The motion character in this case differed from previous hypotheses: the lymphocyte moved within the boundaries of the fiber, sliding along one side or another (fig.7). The stochastic factor was much more prominent than in previous hypotheses. The persistence of motion increased with a higher λ_{chem}. Of the 20 simulations tested, lymphocyte reached the opposite side of the computational domain in 100% cases. On average, the entire fiber transit time spend 16.7 $\pm$ 0.5 min (223 $\pm$ 7 MCS) with the velocity 13.86 $\mu m/min$. To describe the fiber transit times, the mean $\pm$ standard error was calculated. However, a pronounced active cytoskeletal motion, which has a random character, can slow down migration in the gradient direction interfering with the chemotaxis.

For the model based on the fifth hypothesis, a local sensitivity analysis was performed (fig.8). The sensitivity analysis illustrates how variations in separate parameters affect the T cell transit time along the fiber. Predictably, an increase in gradient strength (λ_{chem}) and temperature (T) accelerates T cell gliding along the fiber. For temperature, a different effect sign compared to hypothesis №4 is observed, probably because the intensity of chemotactic and stochastic motion increases, but in 5th model the cell moves within the fiber, as in a corridor, and does not break away from it. It can be assumed that an increase in J_{cf} leads to less adhesion of the T cell to fiber and more intensive gliding, especially when model does not use haptotaxis, and baseline $J_{cm} \gg J_{cf}$, i.e. cell cannot leave fiber. The surface energy of lymphocyte interaction with the environment (J_{cm}), perimeter constraints coefficient λ_{per} and such characteristics of active motion as $\Delta\Theta$, have almost no effect on the transit time. It is interesting that an increase in the energy contribution of active motion to the full Hamiltonian (λ_{Pr}) and persistence of motion (τ) increase the transit time. But an increase in λ_{Pr} probably increases the role of the stochastic component of gliding motion compared to the gradient one and, therefore, can increase the transit time. Increasing τ increases the motion persistence, but on average it does not speed up motion, since protrusive component can be directed in the direction opposite to the chemotactic vector. As in the 4^{th} model, increasing the of the cell rigidity (λ_{Ar}), that is, decreasing compressibility, reliably reduces the gliding speed. And a dummy parameter was introduced to illustrate the intrinsic variability of the simulation results with baseline parameters.

4 Discussion

In order to clarify the purpose of the work, it should be noted that the study was purely theoretical. Systematic calibration on experimental data and validation of the model results were not performed. The

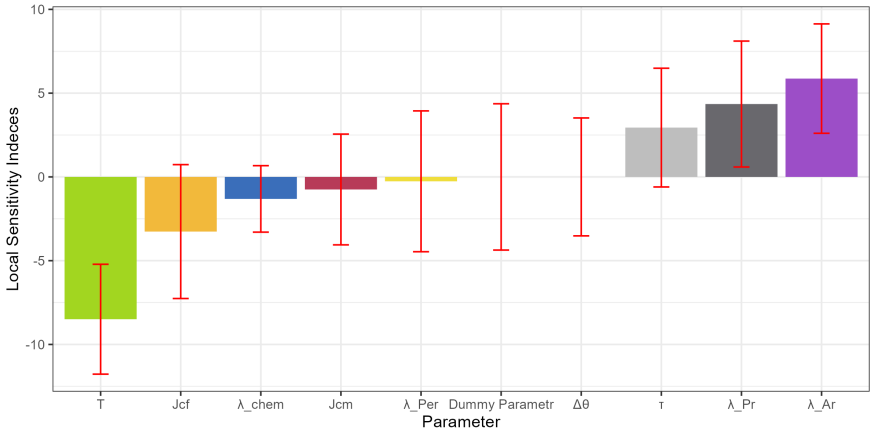

Fig. 8: Local sensitivity analysis of model №5 main parameters variation. The plot shows mean ± se for sensitivity indices based on 40 runs for all parameters (160 runs for λ_{chem}).

only criterion of "success" of the model development was the fact that the most basic requirements of biological plausibility are satisfied during the lymphocyte gliding along the fiber.

Previously, a number of fundamental works were written using the CPM to describe the T cells motion within LNs with the involvement of the RN, where parameters were estimated based on 2-photon measurements.

It was revealed in the experimental study that the constitutive presentation of the CCR7 ligands on the surface of FRC provides important haptokinetic cues to T cells migrating on the FRC network, stimulating the basal intranodal motility of naive T lymphocytes [52]. Imaging adoptively transferred $CD4^+$ T lymphocytes in the paracortical T-zone, a significant reduction of the median of average cell velocities by $\sim$ 33% as well as of the mean motility coefficient by $\sim$ 55% can be observed when comparing the migration behavior of CCR7-deficient and wild type T cells. However, the presented models have not been calibrated on experimental data of two-photon measurements. And in the absence of haptotaxis (or rather, the necessary combination of haptotaxis and chemotaxis), the T cell can stop on the fiber or leave it. Only the first hypothesis (considering hypotheses without haptotaxis) could demonstrate T cell gliding along the entire length of fiber (not in all runs) with average velocity reduction on 58%.

Authors of [53] revealed that T cells walk in a consistent direction for several minutes, pause briefly with a regular period, and then take off in a new, random direction. They constructed a CPM model of T cell and DC migration in LNs and show that all dynamical properties of T cells could be a consequence of the densely packed LN environment. Interestingly, model [53] does not require preferential adhesion of T cells to the RN ($J_{ECM,Tcell} = J_{RN,Tcell} = 5 \times 10^5$), because lymphocytes in their model can move along the extracellular matrix. In the current single-cell model, the role of the ECM is played by the medium, and detachment from the fiber is a sign that the proposed model does not work. All models of the current work use preferential adhesion of T cells to fiber. For example, the next surface energies were used in the fifth model: $J_{ECM,Tcell} = 10, J_{RN,Tcell} = 0$. Also, fiber is modeled here as a single frozen extended structure consisting not of cells but of elementary sites, so there is no surface energy of fibroblasts between each other.

Authors of [54] worked on the question whether T cell chemoattraction towards DCs is expected to promote or hamper the detection of rare antigens using the Cellular Potts Model. Mentioned model contained *in silico* T cells, DCs, RN and the capsule. The latter two elements were included to capture a realistic LN structure. One of numerical results was, that the mean velocity of T cells migrating without chemotactic cues was tuned to about $11.0 \mu m/min$. The mean velocity slightly increased to $12.9 \pm 1.3 \mu m/min$ (17% increase) when T cells migrated chemotactically. Developed model №5 shows a larger difference of T cell velocities with and without chemotaxis than work [54]. Thus, with the use of a chemokine gradient, a T cell transiting a fiber from start to finish covers 1.26 times more pixels (26% increase) with the center of mass than in the absence of a gradient at the same time.

4.1 Novelty of modeling results and used programming tools

Based on previous works [25, 26, 29], an appropriate correction to the Hamiltonian and a computationally easy phenomenological algorithm, that qualitatively reproduce the immune system cells migration along fibronectin fibers due to chemo- and haptotaxis, were chosen. The novelty of the proposed Hamiltonian formalism, that, rejecting non-working hypotheses, it proposes the combinations of haptotaxis and separate components of chemotaxis, which could make the lymphocyte persistently and continuously glide along the fiber. Also, it is worth noting that a universal method was found for numeration of the arbitrary shape fiber sites, which does not require the use of site coordinates and allows fiber representation *via* nonmonotonic function.

The model was built within the framework of the standard CPM modeling approach so that it can be further used in multi-cell calculations, for example, for immune processes taken part in the LNs. Also, in this work, for the first time, the main types of CPM Hamiltonians were implemented in the NetLogo IDE using the cellular automata arsenal at their disposal. There were no such examples neither in the official modeling repository [42], nor in any other published sources [43]. The main advantage of the proposed approach is the following: the implementation of the CPM elements in NetLogo allows implementation of new Hamiltonians proposed in literature [33] and creation of non-standard configurations with lower barrier to entry compared to other ready-to-use tools. On the other hand, in terms of performance, the proposed solution is significantly inferior to ready-for-use software packages for multicellular computing.

The numerical experiments prepared with model revealed the following, the spatial gradient of chemokines is a solution, however not the universal solution of the problem. Also, chemokine concentration distributed along the fiber (haptotaxis) does not solve the problem, at least within the CPM framework. Also, production of chemokines by FRC fibers and their diffusion from the fiber into the lymph is not enough for a satisfactory solution. However, the problem was successfully solved by creating an artificial structure: (1) a linear chemokine concentration gradient along the fiber and (2) a near-surface chemokine layer with a tangentially directed concentration gradient. Possible biological interpretations of such a near-surface chemokine layer around the fiber can be that chemokine held by a "fur coat" of filaments [39, 44].

Additionally, the fifth tested hypothesis demonstrated that the most biologically-relevant reproduction of the lymphocyte migration along the fibers is achieved by allowing stochastic elements in cell migration and integration of an active cytoskeletal motion rather than exploiting random membrane fluctuations. An interesting observation is that long-term motion along a fiber without changing direction, up to passing through it entirely can be observed without involving chemotaxis. This occurs quite rarely and is associated with an increase in correlation between force direction and the direction of the FRC network section, which in fact determines possible directions of the cell migration.

The one of most important result of this computational work is performed exploration of possible Hamiltonian formalism to setup persistent T cell motion along linear fibers within CPM framework. Basing on tested hypotheses any researcher can implement simplified fourth or more complicated fifth type of Hamiltonian into large-scale models of LN T zone. NetLogo programming language is highly optimized for ABM, but not for description of multi-patch figures like biologic cells; it is necessary for CPM to operate with multi-patch figures. Additional implementation problems can be linked with the Java Virtual Machine within NetLogo. Potentially even more computationally optimal models can be built into existing CPM tools, e.g. CompuCell [45], Morpheus [46], Artistoo [47] and Tissue Simulation Toolkit [50], which would allow the use of the lymphocyte's migration model in multicellular large-scale configurations. It should be admitted that in relation to CPM tasks NetLogo is noticeably slower than previous versions of the existing tools, since it was initially optimized for slightly different tasks. The latest version of Morpheus [46] and new packages [57] that use GPU-parallelization work orders of magnitude faster.

However, the final choice was made in favor of NetLogo, firstly, because performance was not a crucial factor for this work – it was the single-cell model. Secondly, it was necessary to be able to manually set complex initial configurations of the computational domain: in the author's experience, this is absent in Morpheus and Artistoo. Thirdly, the ability to deeply edit models using coding using some type of modeling syntaxis was required. Artistoo has a complex JavaScript architecture, which is difficult for ordinary users

to modify. Morpheus writes models in the XML language, but does not allow you to rewrite the code at your own discretion. NetLogo allows deep code modifications, as a flexible Cellular Automata syntaxis that gives commands to separate patches.

4.2 Model limitations and future directions

There are several potential limitations in the current modeling work. First, the fibroblast reticular network is not a linear object, but rather spatial corridors [41]. Attempts to reproduce, as well as search for an algorithm for building a real network, are too complicated and overwhelming to our theoretical study, therefore the present work is limited to linear fragments of the real FRC (for hypotheses 1 – 4). Secondly, we use a 2D framework which significantly simplifies actual three-dimensional FRC network. Thirdly, the computational experiment setup is quite simplified. Instead of solution the reaction-advection-diffusion equation [48] to describe the production of chemokines by the FRC network using a 3D geometric model of this structure, the 2D chemokine fields are generated along one fiber using heuristics-based algorithms. Therefore, the generated chemokine gradient patterns may not reflect the ones observed *in vivo*. Fourthly, the current model is characterized by the fact that the cell membrane does not exist on its own, but only as a boundary of many sites with the same index without elasticity, except for a specific term defined in eq. (3). Therefore, during the testing hypothesis 1 – 4 the creation of polarized cells was not used, and migration was modeled using only minimization of the Hamiltonian, and not due to the cytoskeleton. Fifthly, during the fifth hypothesis testing we were using multiple parameters to describe the most complex of the cell's migration models. In this work, no estimates of the model parameters were made based on experimental data. The parameter values were extracted from literature or arbitrary values were assigned to them that could ensure lymphocyte gliding along the entire length of the fiber. For stochastic models, there is no way to estimate parameters using the Likelihood maximization principle [49]. From the other side massive calculations associated with Approximated Bayesian Computations require high performance computing [49] and are currently not adapted in NetLogo. Sixthly, the work tested 5 hypotheses, but did not consider such more sophisticated mechanisms as (a) focal adhesion dynamics, i.e., integrin-mediated bond formation between the actin bundles and the extracellular fibers [19], (b) cell traction associated with the retrograde actin flow [26], (c) durotaxis, i.e., migration along the gradient of the substrate stiffness [18].

Also, author views separation of the lymphocyte from the FRC fiber as a violation of conditions for successful simulation, although there is nothing unnatural in this phenomenon. Indeed, the fundamental experimental study of 4-dimensional trajectories of T cells moving along FRC network [5, 51] reported that about 10% of cases a T cell can spontaneously separate from the fiber, jump to the adjacent non-intersecting fiber and continue its gliding motion. This discrepancy was largely due to the theoretical character of this work and the task initially set – to test different combinations of Hamiltonians which could support persistent T cell gliding along the fibronectin fiber.

Acknowledgment: This research paper is dedicated to my dear father, who has been nicely my supporter until my research was almost finished and passed away in May 2023. All my early works, as well as this one, were written in constant dialogue with my father, who delved very deeply into any scientific problems and was able to give very valuable practical advice implemented in this work. I am very grateful to all my colleagues at M&S Decisions and the MID3 Research Center at Sechenov University for their continuous support and especially to Dr. Kirill Peskov and Dr. Yuri Kosinsky who helped me a lot with manuscript peer-review and proof-reading. I would also thank Dr. Uri Wilensky (Northwestern University) for providing access to NetLogo 6.3.0. Also, a sincerely appreciate Mikhail Azarov for the help in illustrations preparation for this work.

Supplementary materials NetLogo model files of all five hypotheses, derived data and data visualization scripts can be found on the corresponding GitHub repository page: https://github.com/Potamophylax/CPM_Tcell-FRC.

References

[1] Miller, M. J., Wei, S. H., Parker, I., & Cahalan, M. D. (2002). Two-photon imaging of lymphocyte motility and antigen response in intact lymph node. Science, 296(5574), 1869-1873.

[2] Rey-Barroso, J., Calovi, D. S., Combe, M., German, Y., Moreau, M., Canivet, A., ... & Dupré, L. (2018). Switching between individual and collective motility in B lymphocytes is controlled by cell-matrix adhesion and inter-cellular interactions. Scientific reports, 8(1), 5800.

[3] Textor J, Mandl JN, de Boer RJ (2016) The Reticular Cell Network: A Robust Backbone for Immune Responses. PLoS Biol 14(10)

[4] Bajenoff M, Egen JG, Qi H, Huang AYC, Castellino F, Germain RN. Highways, byways and bread-crumbs: directing lymphocyte traffic in the lymph node. Trends Immunol. 2007; 28: 346–352.

[5] Bajenoff, M., Egen, J. G., Koo, L. Y., Laugier, J. P., Brau, F., Glaichenhaus, N., & Germain, R. N. (2006). Stromal cell networks regulate lymphocyte entry, migration, and territoriality in lymph nodes. Immunity, 25(6), 989-1001.

[6] Graw, F., & Regoes, R. R. (2012). Influence of the fibroblastic reticular network on cell-cell interactions in lymphoid organs. PLoS computational biology, 8(3), e1002436.

[7] Brown, F. D., & Turley, S. J. (2015). Fibroblastic reticular cells: organization and regulation of the T lymphocyte life cycle. The Journal of Immunology, 194(4), 1389-1394.

[8] Ananthakrishnan, R., & Ehrlicher, A. (2007). The forces behind cell movement. International journal of biological sciences, 3(5), 303.

[9] Cucchi, A., Etchegaray, C., Meunier, N., Navoret, L., & Sabbagh, L. (2020). Cell migration in complex environments: chemotaxis and topographical obstacles. ESAIM: Proceedings and Surveys, 67, 191-209.

[10] Mogilner, A. (2009). Mathematics of cell motility: have we got its number?. Journal of mathematical biology, 58, 105-134.

[11] Zhu, J., & Mogilner, A. (2016). Comparison of cell migration mechanical strategies in three-dimensional matrices: a computational study. Interface focus, 6(5), 20160040.

[12] Akiyama, M., Sushida, T., Ishida, S., & Haga, H. (2017). Mathematical model of collective cell migrations based on cell polarity. Development, growth & differentiation, 59(5), 471-490.

[13] Bi, D., Yang, X., Marchetti, M. C., & Manning, M. L. (2016). Motility-driven glass and jamming transitions in biological tissues. Physical Review X, 6(2), 021011.

[14] Moure, A., & Gomez, H. (2021). Phase-field modeling of individual and collective cell migration. Archives of Computational Methods in Engineering, 28, 311-344.

[15] Fletcher, A. G., Osterfield, M., Baker, R. E., & Shvartsman, S. Y. (2014). Vertex models of epithelial morphogenesis. Biophysical journal, 106(11), 2291-2304.

[16] Mohammad, R., Murakawa, H., Svadlenka, K., & Togashi, H. (2021). A level set-based approach for modeling cellular rearrangements in tissue morphogenesis.

[17] Elliott, C. M., Stinner, B., & Venkataraman, C. (2012). Modelling cell motility and chemotaxis with evolving surface finite elements. Journal of The Royal Society Interface, 9(76), 3027-3044.

[18] Rens EG and Merks RM. Cell shape and durotaxis explained from cell-extracellular matrix forces and focal adhesion dynamics. IScience, 23(9):101488, 2020. doi:10.1016/j.isci.2020.101488.

[19] Rens, E. G., & Edelstein-Keshet, L. (2019). From energy to cellular forces in the Cellular Potts Model: An algorithmic approach. PLoS computational biology, 15(12), e1007459.

[20] B Marion, ST Thornton, Classical Dynamics of Systems and particles, Thomson,, 1995.

[21] Kockelkoren, J., Levine, H., & Rappel, W. J. (2003). Computational approach for modeling intra-and extracellular dynamics. Physical Review E, 68(3), 037702.

[22] Hecht I, Skoge ML, Charest PG, Ben-Jacob E, Firtel RA, Loomis WF, Levine H, Rappel WJ (2011) Activated membrane patches guide chemotactic cell motility. PLoS computational biology.

[23] Strychalski W, Copos CA, Lewis OL, Guy RD (2015) A poroelastic immersed boundary method with applications to cell biology. Journal of Computational Physics 282:77–97

[24] Ohta, T., Tarama, M., & Sano, M. (2016). Simple model of cell crawling. Physica D: Nonlinear Phenomena, 318, 3-11.

[25] Guisoni, N., Mazzitello, K. I., & Diambra, L. (2018). Modeling active cell movement with the potts model. Frontiers in Physics,6, 61.

[26] Niculescu, I., Textor, J., & De Boer, R. J. (2015). Crawling and gliding: a computational model for shape-driven cell migration. PLoS computational biology, 11(10), e1004280.

[27] Szabó, A.; Unnep, R.; Méhes, E; Twal, W. O.; Argraves, W. S.; Cao, Y.; Czirók, A. Collective cell motion in endothelial monolayers. Phys. Biology 2010, 7, 046007

[28] Glazier, J. A., & Graner, F. (1993). Simulation of the differential adhesion driven rearrangement of biological cells. Physical Review E, 47(3), 2128.

[29] Savill, N. J., & Hogeweg, P. (1997). Modelling morphogenesis: from single cells to crawling slugs. Journal of theoretical biology, 184(3), 229-235.
[30] Luo, X., Seveau de Noray, V., Aoun, L., Biarnes-Pelicot, M., Strale, P. O., Studer, V., ... & Theodoly, O. (2020). Lymphocytes perform reverse adhesive haptotaxis mediated by LFA-1 integrins. Journal of Cell Science, 133(16), jcs242883.
[31] Lloyd, A. R., Oppenheim, J. J., Kelvin, D. J., & Taub, D. D. (1996). Chemokines regulate T cell adherence to recombinant adhesion molecules and extracellular matrix proteins. Journal of immunology (Baltimore, Md.: 1950), 156(3), 932-938.
[32] Ditlevsen, S., & Samson, A. (2013). Introduction to stochastic models in biology. Stochastic biomathematical models: with applications to neuronal modeling, 3-35.
[33] Guisoni, N., Mazzitello, K. I., & Diambra, L. (2020). Alternating regimes of motion in a model with cell-cell interactions. Physical Review E, 101(6), 062408.
[34] Landau, L. D., & Lifshitz, E. M. (1976). Theoretical physics. Volume 5. Statistical physics. Part 1. book.
[35] Metropolis, N., Rosenbluth, A. W., Rosenbluth, M. N., Teller, A. H., & Teller, E. (1953). Equation of state calculations by fast computing machines. The journal of chemical physics, 21(6), 1087-1092.
[36] Sahni, P. S., Grest, G. S., Anderson, M. P., & Srolovitz, D. J. (1983). Kinetics of the Q-state Potts model in two dimensions. Physical review letters, 50(4), 263.
[37] Mombach, J. C., Glazier, J. A., Raphael, R. C., & Zajac, M. (1995). Quantitative comparison between differential adhesion models and cell sorting in the presence and absence of fluctuations. Physical Review Letters, 75(11), 2244.
[38] Wilensky U. NetLogo. Center for Connected Learning and Computer-Based Modeling. Evanston, IL: Northwestern University. (1999).
[39] Peranzoni, E., Rivas-Caicedo, A., Bougherara, H., Salmon, H., & Donnadieu, E. (2013). Positive and negative influence of the matrix architecture on antitumor immune surveillance. Cellular and molecular life sciences, 70, 4431-4448.
[40] Li, L., Nørrelykke, S. F., & Cox, E. C. (2008). Persistent cell motion in the absence of external signals: a search strategy for eukaryotic cells. PLoS one, 3(5), e2093.
[41] Gretz, J. E., Anderson, A. O., & Shaw, S. (1997). Cords, channels, corridors and conduits: critical architectural elements facilitating cell interactions in the lymph node cortex. Immunological reviews, 156(1), 11-24.
[42] http://ccl.northwestern.edu/netlogo/models/
[43] https://ccl.northwestern.edu/netlogo/models/community/index.cgi
[44] Hara, T., Katakai, T., Lee, J. H., Nambu, Y., Nakajima-Nagata, N., Gonda, H., ... & Shimizu, A. (2006). A transmembrane chemokine, CXC chemokine ligand 16, expressed by lymph node fibroblastic reticular cells has the potential to regulate T cell migration and adhesion. International immunology, 18(2), 301-311.
[45] Swat, M. H., Thomas, G. L., Belmonte, J. M., Shirinifard, A., Hmeljak, D., & Glazier, J. A. (2012). Multi-scale modeling of tissues using CompuCell3D. In Methods in cell biology (Vol. 110, pp. 325-366). Academic Press.
[46] Starruß, J., De Back, W., Brusch, L., & Deutsch, A. (2014). Morpheus: a user-friendly modeling environment for multiscale and multicellular systems biology. Bioinformatics, 30(9), 1331-1332.
[47] Wortel, I. M., & Textor, J. (2021). Artistoo, a library to build, share, and explore simulations of cells and tissues in the web browser. Elife, 10, e61288.
[48] Clairambault, J. (2013). Reaction-Diffusion-Advection Equation. In: Dubitzky, W., Wolkenhauer, O., Cho, KH., Yokota, H. (eds) Encyclopedia of Systems Biology. Springer, New York, NY.
[49] Schälte, Y., & Hasenauer, J. (2020). Efficient exact inference for dynamical systems with noisy measurements using sequential approximate Bayesian computation. Bioinformatics, 36(Supplement 1), i551-i559.
[50] R M H Merks, & J A Glazier. (2005). A cell-centered approach to developmental biology. Physica A, 352(1), 113–130.
[51] Bajénoff, M., Glaichenhaus, N., & Germain, R. N. (2008). Fibroblastic reticular cells guide T lymphocyte entry into and migration within the splenic T cell zone. The Journal of Immunology, 181(6), 3947-3954.
[52] Worbs, T., & Förster, R. (2009). T cell migration dynamics within lymph nodes during steady state: an overview of extracellular and intracellular factors influencing the basal intranodal T cell motility. Visualizing immunity, 71-105.
[53] Beltman, J. B., Marée, A. F., Lynch, J. N., Miller, M. J., & De Boer, R. J. (2007). Lymph node topology dictates T cell migration behavior. The Journal of experimental medicine, 204(4), 771-780.
[54] Vroomans, R. M., Marée, A. F., De Boer, R. J., & Beltman, J. B. (2012). Chemotactic migration of T cells towards dendritic cells promotes the detection of rare antigens. PLOS Computational Biology, 8(11), e1002763.
[55] Graner, F., & Glazier, J. A. (1992). Simulation of biological cell sorting using a two-dimensional extended Potts model. Physical review letters, 69(13), 2013.
[56] Anaya, J. M., Shoenfeld, Y., Rojas-Villarraga, A., Levy, R. A., & Cervera, R. (2013). Autoimmunity: from bench to bedside [Internet].
[57] Sultan, S., Devi, S., Mueller, S. N., & Textor, J. (2023). A parallelized cellular potts model that enables simulations at tissue scale. arXiv preprint arXiv:2312.09317.
[58] Van Liedekerke, P., Palm, M. M., Jagiella, N., & Drasdo, D. (2015). Simulating tissue mechanics with agent-based models: concepts, perspectives and some novel results. Computational particle mechanics, 2, 401-444.